JOURNAL OF GUIDANCE, CONTROL, AND DYNAMICS
Vol. 28, No. 2, March–April 2005

# Low-Thrust Guidance Scheme for Earth-Capture Trajectories

Y. Gao* and C. A. Kluever†
*University of Missouri–Columbia, Columbia, Missouri 65211*

**A new guidance scheme for the Earth-capture phase of a low-thrust spacecraft is developed. The objective of the guidance scheme is to provide the appropriate thrust steering program that will transfer the vehicle from hyperbolic conditions near the Earth's sphere of influence to a circular low-Earth orbit. Blending two control laws that reduce energy and eccentricity, respectively, generates the steering angle commands. The presented guidance design is predictive in nature and does not rely on a stored reference trajectory or reference controls. The guidance algorithm iterates on a single guidance parameter (a blending coefficient) such that a desired performance measure is minimized and boundary conditions are satisfied. Numerical simulations of three-dimensional guided capture trajectories are presented, and results show that the guidance successfully performs the high-energy Earth-capture maneuver. The simplicity of the guidance design makes it a viable candidate for onboard implementation.**

## Introduction

DEEP Space 1 (DS1) demonstrated that solar electric propulsion (SEP) is a viable propulsion option for interplanetary space missions.[1] An interplanetary mission design may include the use of SEP for the Earth-return leg of a sample return mission. For example, Vadali et al.[2] investigated the use of low-thrust propulsion for a Mars sample return mission. In a sample return scenario, SEP would eventually perform the capture maneuver from hyperbolic approach to a closed Earth orbit. It appears that before very recent efforts, research involving optimal SEP capture trajectories was somewhat limited. Battin[3] presented a feasible scheme for performing capture trajectories into a low-lunar orbit with a variable low-thrust engine. Vadali et al.[2] demonstrated a Lyapunov feedback control law for performing a low-thrust capture into a high-altitude Earth elliptical orbit. Recently, Whiffen and Sims[4,5] obtained optimal low-thrust capture trajectories using their static-dynamic control optimization algorithm, and Kluever[6] developed a method for computing optimal low-thrust Earth-capture trajectories. The trajectory optimization method in Ref. 6 simultaneously considered the initial high-energy transfer to a closed orbit and the subsequent quasi-circular spiral transfer (with hundreds of revolutions) to a low-Earth orbit (LEO).

The volume of work involving the low-thrust guidance problem also appears to be somewhat limited. Recently, Petropoulos[7] developed a set of control laws for changing a variety of orbital elements that may be suitable for a low-thrust guidance algorithm. Low-thrust guidance may be defined as the determination of the thrust-steering program that is required to attain a target orbit. This guidance problem presents a challenge because the thrust magnitude is small (SEP thrust-to-weight ratio is typically around $10^{-5}$–$10^{-4}$) and the continuous steering commands must be determined over a long transfer time (possibly hundreds of days). In addition, trajectory optimization methods typically determine an open-loop steering program that may be difficult or impractical to store onboard for use by a guidance system. Furthermore, the low control authority characteristic of SEP may preclude the use of traditional path-following guidance designs that rely on a single stored control and trajectory reference profile.

Presented as Paper 2003-639 at the AAS/AIAA Astrodynamics Specialist Conference, Big Sky, MT, 3 August 2003; received 22 August 2003; revision received 9 March 2004; accepted for publication 9 March 2004. 

*Graduate Research Assistant, Mechanical and Aerospace Engineering Department; yg386@mizzou.edu.

†Associate Professor, Mechanical and Aerospace Engineering Department; KlueverC@missouri.edu. Associate Fellow AIAA.

Simplicity, reliability, and autonomy are all desirable characteristics of a good guidance design. Desai et al.[8] developed an autonomous guidance system for DS1 that targeted flyby conditions with an asteroid and a comet. The DS1 guidance computed steering corrections based on a linear combination of deviations between a reference (stored) target state and a numerically projected trajectory. This linear guidance design was used only for small trajectory deviations (small steering corrections); significant deviations required a complete redesign of the reference trajectory and steering profiles, which was performed on the ground.

In this paper, we present a new predictive guidance scheme for performing an Earth-capture maneuver using low-thrust propulsion. We assume that the capture trajectory begins with hyperbolic conditions near the Earth's sphere of influence (SOI) and that the terminal target is a circular LEO. Our guidance design is composed of two major stages. The first phase reduces orbital energy and eccentricity to establish a closed orbit at the first perigee passage. The second guidance phase reduces energy, eccentricity, and inclination so that the resulting trajectory terminates on a surface defined by universal low-thrust planar spiral trajectory solutions.[9] Once the spacecraft has reached the spiral solution surface, a simple thrust-steering profile (such as antivelocity steering) can be used to guide the vehicle on an inward winding spiral path to the target LEO. Both initial guidance phases alter the capture trajectory by adjusting a single guidance parameter. Numerical results are presented for the guided capture trajectories.

## System Model

The Earth-capture trajectory is governed by the following dynamic equations:

$$\frac{\mathrm{d}\boldsymbol{r}}{\mathrm{d}t} = \boldsymbol{v} \tag{1}$$

$$\frac{\mathrm{d}\boldsymbol{v}}{\mathrm{d}t} = \frac{-\mu \boldsymbol{r}}{r^3} + \boldsymbol{a}_P + \boldsymbol{a}_T \tag{2}$$

$$\frac{\mathrm{d}m}{\mathrm{d}t} = \frac{-2\eta P}{(g I_{\mathrm{sp}})^2} \tag{3}$$

where $\boldsymbol{r}$ and $\boldsymbol{v}$ are the position and velocity vectors of the spacecraft in an Earth-centered inertial (ECI) Cartesian frame, $\mu$ is the Earth gravitational constant, $\boldsymbol{a}_P$ is an acceleration vector due to perturbations, and $\boldsymbol{a}_T$ is the thrust acceleration vector. Equation (3) defines the mass loss due to the low-thrust engine where $m$ is spacecraft mass, $P$ is input power to the SEP system, $\eta$ is engine efficiency, $g = 9.80665\ \mathrm{m/s^2}$ is Earth's gravitational acceleration, and $I_{\mathrm{sp}}$ is specific impulse. Perturbation vector $\boldsymbol{a}_P$ in Eq. (2) accounts for Earth oblateness ($J_2$) and lunar and solar effects. Lunar and solar gravitational accelerations are computed by the use of Cowell's method

(see Ref. 10), where lunar and solar positions are defined by inertially fixed elliptical orbits for the moon and Earth with respect to ECI and heliocentric frames, respectively. Thrust acceleration $\boldsymbol{a}_T$ in the ECI frame is

$$\boldsymbol{a}_T = (2\eta P/mgI_{\text{sp}})\hat{\boldsymbol{u}}_{\text{ECI}} \tag{4}$$

where $\hat{\boldsymbol{u}}_{\text{ECI}}$ is a unit vector along the thrust direction. It is advantageous to define the thrust-direction unit vector in a local-vertical/local-horizontal (LVLH) frame in terms of local pitch and yaw steering angles:

$$\hat{\boldsymbol{u}}_{\text{LVLH}} = [\sin\alpha\cos\beta \quad \cos\alpha\cos\beta \quad \sin\beta]^T \tag{5}$$

Pitch angle $\alpha$ is measured from the local horizon to the projection of the thrust vector onto the orbit plane, and yaw angle $\beta$ is measured from the orbit plane to the thrust vector. A coordinate transformation from the LVLH to ECI frame determines the thrust direction required in Eq. (4).

## Capture Guidance Scheme

The goal of the guidance design is to determine the thrust-steering angle program such that the vehicle will follow a capture trajectory to circular LEO. It is assumed that the SEP vehicle is on a return path to Earth (perhaps the end of a sample return mission), and the capture phase begins near the Earth's SOI with hyperbolic conditions with respect to the Earth's gravity field.

We choose to develop a predictive guidance system instead of a path-following guidance design that relies on a stored reference trajectory. Furthermore, we wish to keep our guidance design simple, and, therefore, the scheme determines the steering-angle commands by selection of a single guidance parameter. The capture guidance is separated into three basic phases: 1) initial energy and eccentricity reduction, 2) transition to spiral boundary surface, and 3) spiral transfer to target LEO.

### Initial Energy and Eccentricity Reduction Guidance Phase

The goal of the initial guidance phase is to reduce orbital energy and eccentricity such that a closed (elliptic) orbit is established at the first perigee passage. Our initial guidance phase accomplishes this task by blending two individual control laws that, respectively, reduce the energy and eccentricity as quickly as possible. We assume that no out-of-plane (yaw) steering is employed, so that all propulsive force can be used to alter orbital energy and eccentricity. A desired inclination-change maneuver can be efficiently performed at nodal crossings after a closed orbit is established. The first control law, which minimizes the rate of energy change, is derived from the governing energy-rate equation

$$\frac{\mathrm{d}E}{\mathrm{d}t} = a_T\sqrt{\frac{\mu}{p}}[e\sin\theta\sin\alpha + (1+e\cos\theta)\cos\alpha] \tag{6}$$

where $E$ is orbital energy, $p$ is the semilatus rectum, $e$ is eccentricity, and $\theta$ is true anomaly. Optimal pitch steering that minimizes energy rate is determined by setting the partial derivative of Eq. (6) equal to zero:

$$\frac{\partial\dot{E}}{\partial\alpha} = a_T\sqrt{\frac{\mu}{p}}[e\sin\theta\cos\alpha - (1+e\cos\theta)\sin\alpha] = 0 \tag{7}$$

The resulting extremal control law is

$$\tan\alpha = e\sin\theta/(1+e\cos\theta) \tag{8}$$

The optimal control law that minimizes energy rate is determined by the use of the second partial derivative of Eq. (6) and selection of the proper sign to ensure that $\partial^2\dot{E}/\partial\alpha^2 \geq 0$. The optimal control law is

$$\sin\alpha = \frac{-e\sin\theta}{\sqrt{1+e^2+2e\cos\theta}} \tag{9}$$

$$\cos\alpha = \frac{-(1+e\cos\theta)}{\sqrt{1+e^2+2e\cos\theta}} \tag{10}$$

This control law aligns the thrust vector in the opposite direction of the instantaneous velocity vector (antitangent steering).

The second control law reduces eccentricity during the capture maneuver. Eccentricity can be determined from orbital energy and angular momentum $h$:

$$e = \sqrt{1+(2Eh^2/\mu^2)} \tag{11}$$

At the start of the Earth-capture phase (near the SOI), the orbit is hyperbolic with eccentricity slightly greater than one and energy slightly positive. The velocity vector may be nearly aligned with the radial direction. Therefore, antitangent steering will reduce energy to some extent, but the subsequent orbit will approach a degenerate conic where kinetic energy is due entirely to radial velocity and perigee radius is zero. To avoid this degenerate case, the thrust acceleration must have a component in the horizontal direction to increase angular momentum. Equation (11) shows that increasing $h$ after a capture orbit is established ($E<0$) decreases eccentricity. Therefore, the simple inertial thrust-steering control law is proposed:

$$\alpha = \pi + \theta, \qquad -\pi \leq \theta < 0 \text{ rad} \tag{12}$$

Control law (12) fixes the thrust vector perpendicular to the line of apses, so that angular momentum is increased when the spacecraft is near apogee. Steering law (12) is essentially the inertial-fixed steering program for decreasing eccentricity proposed by Spitzer for Earth orbit-raising maneuvers.[11]

The blended steering direction is determined from a linear combination of the minimum-energy rate and inertial steering programs

$$\hat{\boldsymbol{u}} = \hat{\boldsymbol{u}}_E + \lambda\hat{\boldsymbol{u}}_I \tag{13}$$

where $\lambda$ is a constant scalar that is updated at regular intervals. Unit vectors $\hat{\boldsymbol{u}}_E$ and $\hat{\boldsymbol{u}}_I$ are the thrust directions for the minimum-energy rate and inertial steering control laws, respectively, as regulated by Eqs. (9), (10), and (12). The respective thrust-direction unit vectors in the LVLH frame are determined by Eq. (5), with the appropriate pitch angle and zero yaw angle ($\beta = 0$).

The initial guidance phase adjusts the single guidance parameter $\lambda$ so that a desirable closed orbit is established at the first perigee passage. Desirable orbital conditions at perigee are low eccentricity and radius greater than some acceptable lower bound ($r_{\text{min}}$). Therefore, the guidance scheme selects the best parameter $\lambda$ by minimizing the following augmented performance index

$$J = e_p + \Phi(r_p) \tag{14}$$

where $e_p$ and $r_p$ are eccentricity and radius at perigee, respectively. The penalty function $\Phi(r_p)$ is

$$\Phi(r_p) = \begin{cases} 0 & \text{if} \quad r_p \geq r_{\text{min}} \\ A(r_{\text{min}} - r_p) & \text{if} \quad r_p < r_{\text{min}} \end{cases} \tag{15}$$

where $A$ is a positive penalty function constant. The guidance algorithm predicts the capture trajectory by numerically integrating the planar two-body equations of motion from the current state to the predicted perigee passage. Numerical integration by the guidance scheme is performed by a fourth-order, fixed-step Runge–Kutta routine. Thrust steering during the capture is solely determined by the guidance constant $\lambda$. Therefore, shooting several trajectories to perigee for a range of $\lambda$ values and sorting the resulting values of performance index $J$ performs a simple one-dimensional minimization search. This simple minimization approach uses a two-stage approach, with an initial coarse search followed by a refined search on a smaller grid of $\lambda$ values. The first search involves six $\lambda$ values equally distributed from 0 to 5, and six trajectories are propagated to perigee. Next, a refined search is performed by the use of a finer grid of six $\lambda$ parameters that are equally distributed about the minimizing value from the initial coarse search. Once an optimal $\lambda^*$ is determined after the second stage, then it is held constant and the true spacecraft trajectory is propagated forward by numerical integration of Eqs. (1–3), which include perturbations due to

oblateness and lunar and solar gravitational forces. Thrust steering is determined by $\lambda^*$ and Eq. (13) during integration of the true trajectory. The guidance parameter $\lambda$ is updated at regular intervals by re-solving the one-dimensional minimization problem with the two-stage trajectory shooting approach. We refer to re-solving the minimization problem as the guidance update for parameter $\lambda$. The initial guidance phase ends when the spacecraft reaches perigee.

**Spiral Target Guidance Phase**

The goal of the second phase is to guide the spacecraft to a target energy–eccentricity state defined by acceptable inward spiral trajectories. Although the initial guidance phase will establish a closed orbit at first perigee passage, eccentricity and energy (and, therefore, apogee radius) will be quite high. A trajectory with a high apogee radius and large eccentricity will be perturbed by lunar and solar gravity, which will complicate trajectory planning and guidance calculations. Therefore, a robust guidance strategy would be to establish a nearly circular high-altitude orbit, so that the low-thrust spacecraft can subsequently follow a quasi-circular inward spiral transfer to LEO by the use of a simple antitangent thrust-steering program. Such a steering and trajectory profile is easy to implement and would provide nearly autonomous operation for the majority of the transfer to LEO.

The target boundary state is derived from Perkins's set of universal low-thrust spiral trajectory solutions, which hold for a wide range of thrust-to-weight ratios.[9] Perkins[9] developed universal solutions for low-thrust planar spiral transfers with a constant, continuous thrust force aligned with the velocity vector, that is, tangent steering. Perkins's solutions for dimensionless velocity magnitude $V$, flight-path angle $\gamma$, and dimensionless time parameter $T$ are presented in Fig. 1 with dimensionless radial distance $R$ as the independent variable. If an inward spiral trajectory is desired, then the flight-path angle from Fig. 1b is set as a negative value. Dimensionless time parameter $T$ is the time beyond local escape conditions, and, therefore, the vertical dashed line with $T = 0$ indicates local escape (parabolic orbit) conditions. Dimensional values of radius, velocity magnitude, and spiral time to a point on the unwinding (or, inward winding) spiral can be computed from the dimensionless values ($R$, $V$, and $T$) and the appropriate scaling equations that involve the central body gravitational parameter, initial circular orbit radius, and thrust-to-weight ratio. (See Refs. 6 and 9 for details.)

The target spiral boundary for the second guidance phase is the energy–eccentricity phase plane that can be mapped from Perkins's universal spiral solutions presented in Fig. 1. A specific energy–eccentricity state can be determined from the values for radius, velocity magnitude, and flight-path angle that exist on the universal spiral trajectory. Figure 2 shows the energy–eccentricity space mapped from Perkins's spiral solutions. (Energy has been transformed to dimensional units by the use of the Earth's gravitational parameter, initial LEO, and initial thrust-to-weight ratio.) The curve presented in Fig. 2 represents the osculating values of energy and eccentricity that exist on an outward or inward winding spiral trajectory. At the first perigee passage, the vehicle will have an energy–eccentricity state in Fig. 2 that is below the zero-energy horizontal line and to the left of the unity–eccentricity vertical line.

The second guidance phase blends two optimal control laws (minimum energy- and eccentricity-rate steering programs) so that the predicted capture trajectory terminates on the spiral target boundary presented by Fig. 2. Minimum eccentricity-rate steering is derived from the governing equation for eccentricity

$$\frac{\mathrm{d}e}{\mathrm{d}t} = a_T \sqrt{\frac{p}{\mu}} [\sin\theta \sin\alpha + (\cos\theta + \cos\psi)\cos\alpha] \tag{16}$$

where $\psi$ is eccentric anomaly. By the use of the derivation for minimum energy-rate steering, the first derivative $\partial \dot{e}/\partial\alpha$ is set to zero, and a positive second derivative is ensured. The resulting optimal control for minimum eccentricity rate is

$$\sin\alpha = \frac{-\sin\theta}{\sqrt{1 + 2\cos\theta\cos\psi + \cos^2\psi}} \tag{17}$$

$$\cos\alpha = \frac{-(\cos\theta + \cos\psi)}{\sqrt{1 + 2\cos\theta\cos\psi + \cos^2\psi}} \tag{18}$$

The blended steering direction is determined from a linear combination of the minimum energy-rate and minimum eccentricity-rate steering programs

$$\hat{\boldsymbol{u}} = \hat{\boldsymbol{u}}_E + \lambda \hat{\boldsymbol{u}}_e \tag{19}$$

Unit vectors $\hat{\boldsymbol{u}}_E$ and $\hat{\boldsymbol{u}}_e$ are the thrust directions for the minimum energy- and eccentricity-rate control laws, respectively. Similar to the preceding phase, the second guidance phase adjusts guidance parameter $\lambda$, so that the predicted trajectory terminates on the spiral boundary shown in Fig. 2. Because several values of $\lambda$ will lead to interception with the desired energy–eccentricity boundary curve, the guidance scheme selects the best $\lambda$ by minimization of

$$J = t_{\text{spiral}} \tag{20}$$

where $t_{\text{spiral}}$ is the subsequent inward spiral time to LEO (moving along the curve in Fig. 2) as predicted by Perkins's universal spiral solutions. As before, the test of a range of $\lambda$ values by employment of a two-stage trajectory shooting method solves this one-dimensional minimization problem. Robustness is improved by the exclusion of $\lambda$ values that do not produce trajectories that reach the boundary curve before a specified lower energy threshold. If all $\lambda$ values produce trajectories that do not reach the Perkins's boundary curve before the designated lower energy threshold, then the candidate trajectory with the lowest eccentricity at the energy threshold is selected. (Recall that $\lambda$ is periodically updated, and so the later update trials will produce trajectories that reach the Perkins boundary.)

During the initial guidance phase, no out-of-plane (yaw) steering is employed because we want to establish a closed obit at the first perigee pass. However, it is possible to perform a desired plane change during the spiral target guidance phase and terminate on the Perkins's boundary curve. The yaw-steering guidance can be determined by consideration of the variational equations for inclination and argument of perigee

$$\frac{\mathrm{d}i}{\mathrm{d}t} = \frac{r}{\sqrt{\mu p}} \cos(\omega + \theta) a_T \sin\beta \tag{21}$$

$$\frac{\mathrm{d}\omega}{\mathrm{d}t} = -\frac{1}{e}\sqrt{\frac{p}{\mu}} a_T \left[ \cos\theta \sin\alpha - \left(1 + \frac{r}{p}\right) \sin\theta \cos\alpha \right] \tag{22}$$

where $i$ is the orbital inclination, $r$ is the radial distance, and $\omega$ is the argument of perigee. Obviously, the inclination rate is maximized when the yaw steering angle is $\beta = \pm\pi/2$. Furthermore, the inclination rate is maximized when $r$ is large (apogee) and when the spacecraft is at a nodal crossing (longitude angle $\omega + \theta = 0$ or $\pi$). However, the nodal crossing may not coincide with apogee, and so the argument of perigee profile must be obtained to find the orbital location for maximum inclination rate. Therefore, the guidance scheme numerically integrates Eq. (22) to propagate the argument of perigee. This auxiliary propagation is performed after the optimal $\lambda^*$ value is determined via the planar propagation to the Perkins boundary. (Recall that the initial propagation and search for $\lambda^*$ is completely planar.) Propagation of Eq. (22) is straightforward because the planar states and pitch angle histories are known. After $\omega(t)$ is propagated forward in time, the switch time $t^*$ that produces the maximum inclination rate can be determined from Eq. (21). Time $t^*$ determines when to switch from in-plane (pitch) steering to out-of-plane (yaw) steering.

Once the optimal $\lambda^*$ and $t^*$ are determined, the true trajectory is determined by numerical integration of Eqs. (1–3) with the pitch steering program determined by Eq. (19). When time reaches the predicted switch time $t^*$, the yaw angle is stepped to $\pm\pi/2$ (sign depends on cosine of longitude) and pure yaw steering is employed until the desired plane change is performed. Note that the energy–eccentricity state will (theoretically) remain at a fixed point in Fig. 2 for two-body motion with purely out-of-plane thrust. The

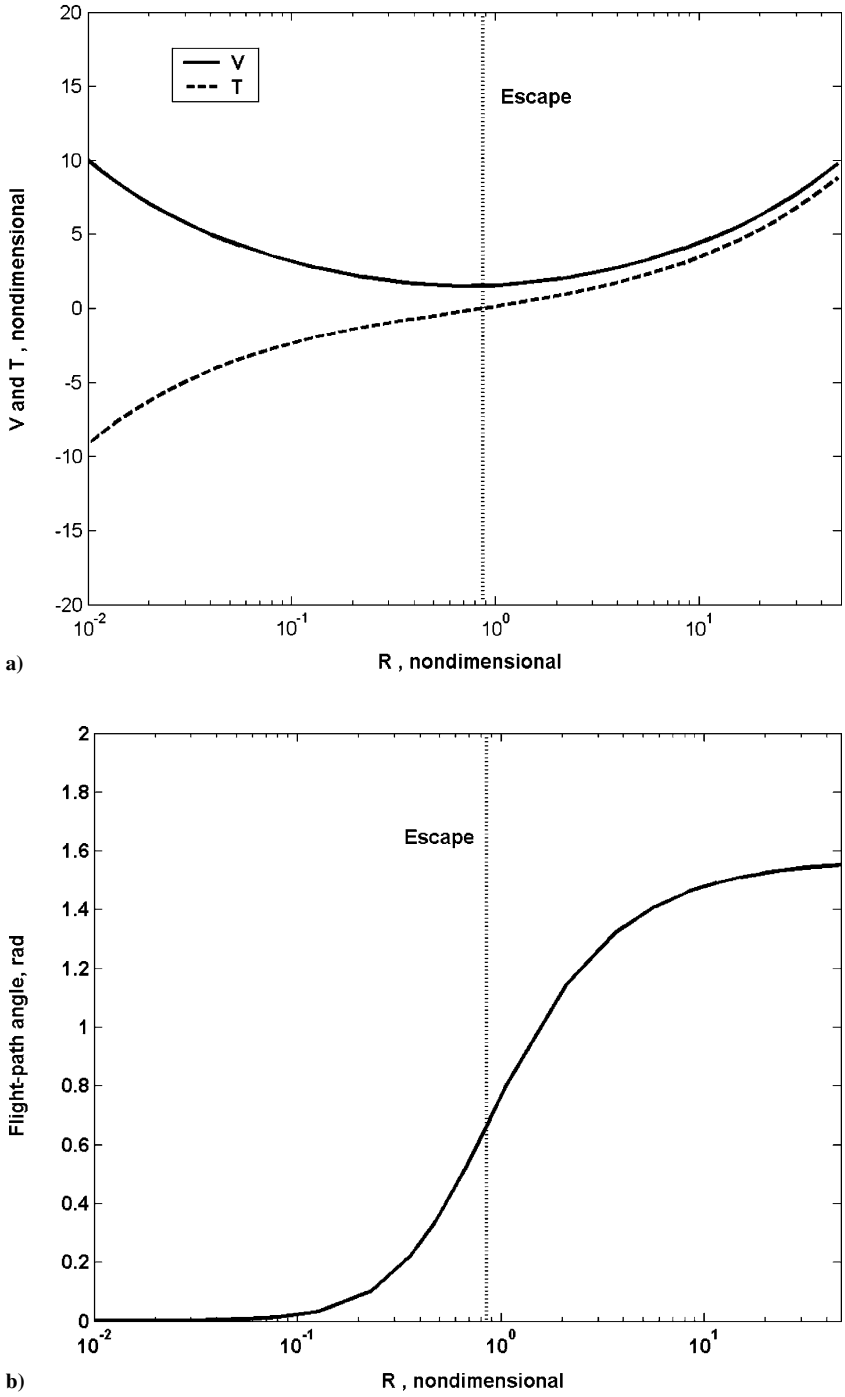


**Fig. 1 Perkins's low-thrust spiral solutions: a) velocity and spiral time and b) flight-path angle.[9]**

need to propagate $\omega$ is eliminated once the spacecraft begins the yaw-steering phase, and $\beta$ is set to zero when the plane change is accomplished. As with the first guidance phase, the parameter $\lambda$ is periodically updated until the vehicle reaches the spiral target boundary. The osculating values of energy and eccentricity are monitored, and the spiral target guidance phase is terminated when the energy–eccentricity state intercepts the boundary presented in Fig. 2.

**Inward Spiral Guidance Phase**

The third guidance phase begins on the spiral target boundary, or an energy–eccentricity state defined by Fig. 2. However, the spacecraft may not be in the proper orbital position to begin following the inward spiral trajectory defined by Perkins's solution. Therefore, the vehicle may need to coast to the appropriate true anomaly (between apogee and perigee) such that the flight-path angle $\gamma$ matches the appropriate value for the given orbital energy [determined by an $(R, V)$ combination in Fig. 1a]. Once the vehicle has reached the appropriate (negative) flight-path angle, the inward spiral guidance may employ a simple antitangent thrust steering program for the majority of the trajectory to LEO. (Recall that Perkins's universal solutions are unwinding spirals with tangential thrust.) If a plane change is required, then a simple yaw steering strategy may be employed during the inward spiral. For example, nominal out-of-plane steering could be commanded near nodal crossings to change orbital inclination, and the amplitude of the yaw steering angle could be reduced as the inclination error and orbital radius decrease.

Perkins's universal low-thrust solutions predict the inward spiral time, but these solutions assume uninterrupted continuous thrust. An SEP vehicle will experience increasing periods of Earth-shadow conditions (with total loss of thrust) as the orbital energy decreases.

Shadow eclipses produce asymmetric thrusting arcs that result in residual eccentricity as the spacecraft approaches the orbital energy for LEO. Therefore, a terminal guidance steering strategy should be employed near LEO, so that eccentricity can be reduced simultaneously with orbital energy.

## Numerical Results

We present numerical simulations to demonstrate the proposed capture guidance scheme. The initial condition for the Earth-capture trajectory is taken from the latter stage of a minimum-propellant Mars–Earth transfer, which could be the return phase of a low-thrust sample return mission. The initial Earth-relative spacecraft state is determined by the difference between the heliocentric position and velocity vectors of the spacecraft and Earth, and Table 1 presents this state.[6] Note that the initial flight-path angle is $\gamma_0 = -85.79$ deg, for a nearly radial descent trajectory. Note that this initial state is from a low-thrust Mars–Earth transit where only the heliocentric phase has been optimized. Furthermore, end-to-end optimization (which includes optimizing the planetary escape and capture arcs) will likely produce an initial Earth-relative flight path that is not radial. Whiffen and Sims[4,5] have solved end-to-end trajectory optimization problems that include the escape and capture spirals.

Initial spacecraft mass is $m_0 = 315$ kg. The constant spacecraft system parameters are $P = 3$ kW, $\eta = 0.68$, and $I_{sp} = 3800$ s, which represent the current level of SEP technology. Numerical integration of the trajectory dynamics [Eqs. (1–3)] is performed by a fourth-order Runge–Kutta method with a variable integration step. Both absolute and relative error tolerances are set as $10^{-8}$ in nondimensional time units, and the states are recorded every 13.45 min.

**Table 1 Initial spacecraft state for capture trajectory**

| Parameter | Value |
|---|---|
| $\boldsymbol{r}_0$ | $[-1.9376(10^5) \quad -9.6272(10^5) \quad -1.0861(10^6)]^T$ km |
| $\boldsymbol{v}_0$ | $[0.1924 \quad 0.6384 \quad 0.6866]^T$ km/s |
| $E_0$ | 0.1858 km$^2$/s$^2$ |
| $e_0$ | 1.0123 |
| $\gamma_0$ | −85.79 deg |
| $i_0$ | 53.28 deg |
| $\Omega_0$ | 23.08 deg |
| $\theta_0$ | 194.09 deg |
| Date at SOI | 18 Aug. 2014 |

The powered capture begins with the initial energy and eccentricity reduction guidance phase, and the guidance update period for $\lambda$ is 4.67 days. A lower perigee radius bound $r_{\min}$ is set at 20 Earth radii. Figure 3 presents the results of the (second) refined search stage for each $\lambda$ update cycle. Note that the optimal $\lambda^*$ decreases with each update as the spacecraft approaches the first perigee passage, and that the predicted eccentricity at perigee changes between update periods. The last $\lambda$ update cycle (update four) results in an optimal $\lambda^*$ that is nearly zero, and, therefore, the thrust vector is essentially opposite the velocity vector [c.f. Eq. (13)] until the spacecraft reaches perigee. The variation in predicted eccentricity is due to the solar and lunar gravitational perturbations because the onboard guidance algorithm utilizes a two-body model for simplicity and computational efficiency. The spacecraft reaches perigee in 15.69 days, and resulting eccentricity is 0.847 at perigee.

Several initial capture trajectories were simulated for a range of update cycle periods, and the results are listed in Table 2. The value in the last column, $t_{G1}$, is the duration of the first guidance phase and the flight time from the SOI to perigee. The initial capture phase appears to be relatively insensitive to the $\lambda$ update frequency. (Note that the last Table 2 entry involves only a single $\lambda$ update during the capture.) Eccentricity at perigee is consistently around 0.85, and the time to perigee is around 15.7 days. Perigee radius approaches the lower boundary of 20 Earth radii because the update cycle frequency increases; therefore, a high $\lambda$ update rate may be necessary if a particular target perigee radius is desired.

Figure 4 shows an event timeline for the spiral target guidance phase, which is initiated at the first perigee pass, when the flight time from SOI is 15.7 days. Note that the $\lambda$ update cycle is $\Delta t = 9.33$ days and the transit time of the second guidance phase is $t_{G2}$. Figure 5 shows the predicted trajectories in the energy–eccentricity space for $\lambda$ test values (for the second refined search stage), as computed by

**Table 2 Initial capture trials with various guidance update frequencies**

| Update period, days | Eccentricity at perigee | Energy at perigee, km$^2$/s$^2$ | Perigee radius, Earth radii | $t_{G1}$, days |
|---|---|---|---|---|
| 0.93 | 0.8499 | −0.2269 | 20.17 | 15.669 |
| 1.87 | 0.8494 | −0.2259 | 20.31 | 15.669 |
| 3.73 | 0.8480 | −0.2181 | 21.16 | 15.679 |
| 4.67 | 0.8472 | −0.2164 | 22.06 | 15.688 |
| 9.33 | 0.8478 | −0.2122 | 22.41 | 15.688 |

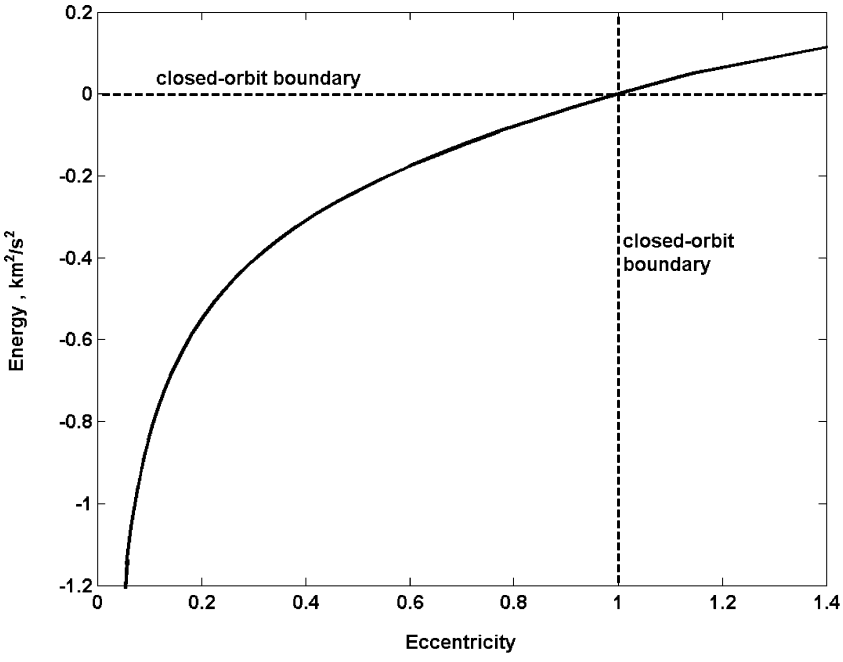


**Fig. 2 Perkins's low-thrust spiral solutions in energy–eccentricity space.[9]**

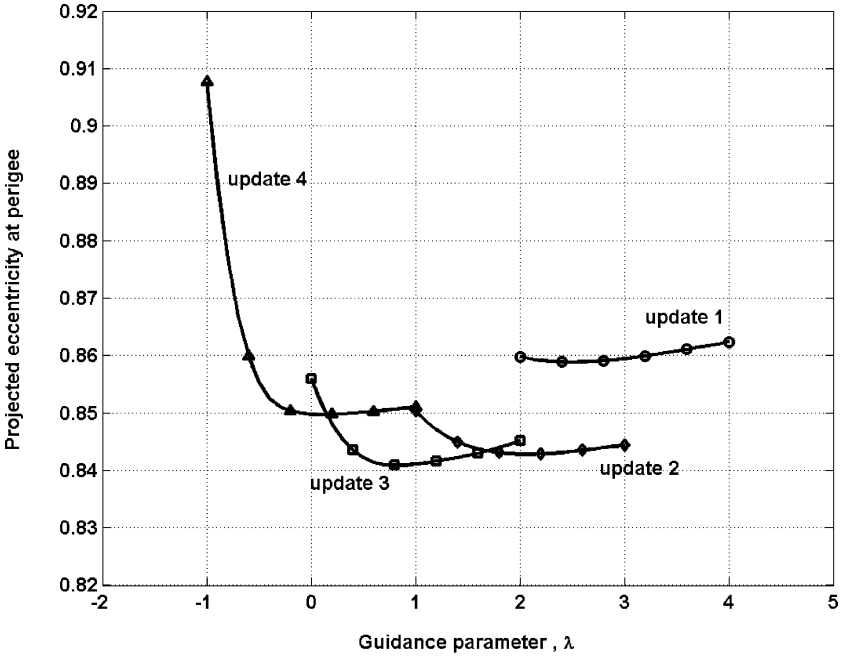


**Fig. 3 Projected eccentricity at perigee for guidance parameter $\lambda$ update trials.**

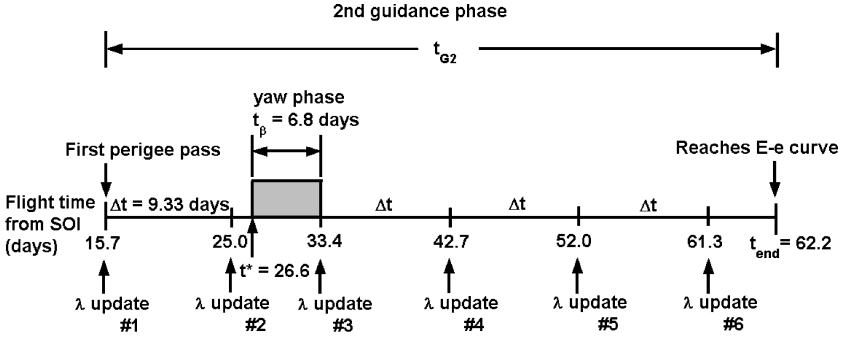


**Fig. 4 Event timeline for $\lambda$ update cycles for the second guidance phase.**

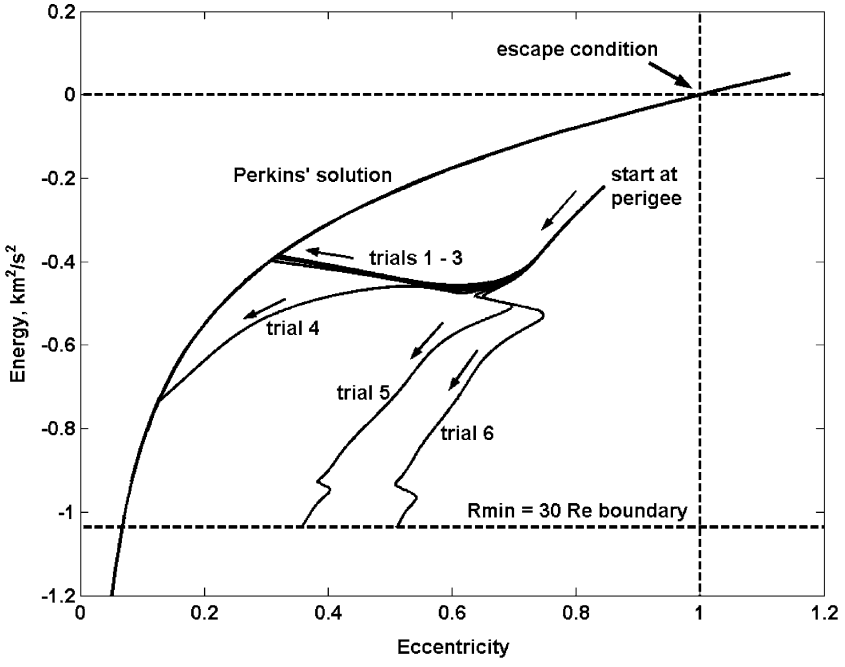


**Fig. 5 Guidance parameter $\lambda$ update trials at start of second guidance phase.**

**Table 3 Second guidance phase trials with various energy (radius) thresholds**

| $R_{\min}$, $Re$ | $r_{\text{end}}$, $Re$ | $e_{\text{end}}$ | $\theta_{\text{end}}$, deg | $\theta_{\text{spiral}}$, deg | $t_\beta$, days | $i_{\text{end}}$, deg | $t_{G2}$, days | $t_{\text{coast}}$, days | $t_{\text{spiral}}$, days |
|---|---|---|---|---|---|---|---|---|---|
| 50 | 43.63 | 0.140 | 341.3 | 276.9 | 6.90 | 28.36 | 34.5 | 15.23 | 197.0 |
| 40 | 37.59 | 0.106 | 119.1 | 276.0 | 6.81 | 28.55 | 37.2 | 6.91 | 194.0 |
| 30 | 30.77 | 0.071 | 337.3 | 272.1 | 6.81 | 28.31 | 46.5 | 8.28 | 189.8 |
| 20 | 22.38 | 0.038 | 117.4 | 272.4 | 6.81 | 28.36 | 54.9 | 2.88 | 182.1 |
| 10 | 10.03 | 0.008 | 3.3 | 277.2 | 10.45 | 28.55 | 91.3 | 1.43 | 156.8 |

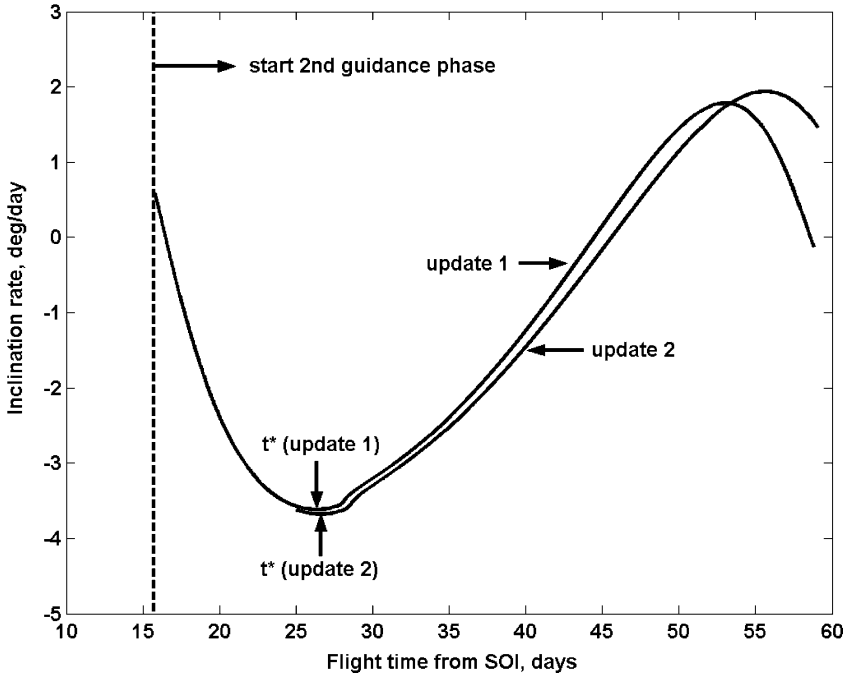


**Fig. 6 Predicted inclination rate for two update cycles in second guidance phase.**

the onboard guidance scheme. Figure 5 shows the first shooting trials to select the optimal λ as the second guidance phase is initiated. The lower energy bound is set at $-1.0416\ \text{km}^2/\text{s}^2$, that is, the corresponding energy from Perkins's solution when $R = 30$ Earth radii, and, therefore, test trajectories five and six are discarded during the shooting trials because they do not reach Perkins's spiral trajectory curve before this energy threshold. Shooting trial four results in the minimum predicted spiral time $t_{\text{spiral}}$, and, therefore, the respective λ value is used for the initial steering program until the next update cycle.

Once the optimal $\lambda^*$ and propagated planar trajectory is obtained, the guidance computes the time $t^*$ when the inclination rate is maximized. Figure 6 shows the time history of the predicted inclination rate using the optimal $\lambda^*$ and the propagated planar trajectory from the first shooting trial. Figure 6 shows that the predicted $t^*$ for maximum negative $\text{d}i/\text{d}t$ is about 26 days for the first update cycle (at the start of the second guidance phase). The event timeline presented in Fig. 4 shows that the second λ update cycle occurs at $t = 25.0$ days, and, therefore, $t^*$ is recomputed during the second update cycle, and the updated $t^*$ is slightly greater than its first estimate (Fig. 6). Once the yaw-steering phase is initiated at $t^* = 26.6$ days, thrust is directed normal to the orbit plane for a duration of $t_\beta = 6.8$ days (Fig. 4). When the yaw phase is completed at $t = 33.4$ days, guidance reinitiates the λ update cycle and ceases to propagate Eq. (22) and predict the inclination rate. Figure 4 shows that four additional λ update cycles are performed before the spacecraft reaches the energy–eccentricity boundary at $t = 62.2$ days.

Table 3 lists the performance of the second guidance phase for a range of lower-energy threshold values. (Energy threshold from the Perkins solution is presented in terms of radius $R_{\min}$.) All trajectory results use a nominal 9.33-day update period for λ. The subscript "end" denotes orbit parameters pertaining to the energy–eccentricity curve intersection point. Note that, in each case, the spacecraft intersects the energy–eccentricity curve at a radial distance that is close to the respective lower bound on energy (radius). This characteristic demonstrates that the update scheme is driving the vehicle to the lowest possible energy–eccentricity state to minimize the subsequent inward spiral time. Eccentricity at the target spiral intersection is also presented in Table 3, and the initial inward spiral becomes more circular as the energy threshold is decreased. Table 3 also presents the true anomaly of the spacecraft at the boundary curve intersection ($\theta_{\text{end}}$), as well as the true anomaly required for proper initiation of the inward spiral ($\theta_{\text{spiral}}$). Recall that the energy–eccentricity boundary curve in Fig. 2 merely defines the instantaneous size and shape of the orbit for the initiation of an inward spiral trajectory without regard for position in the orbit. Orbital position is dictated by the respective flight-path angle (shown in Fig. 1b), with the proper quadrant determined by the sign of $\gamma$ (outward or inward spiral). The guided trajectories for $R_{\min} = 40$ and 20 Earth radii intersect the boundary curve such that the subsequent coast angle is less than 180 deg, and, therefore, a relatively short coast phase $t_{\text{coast}}$ is needed before the vehicle has the proper radius, velocity, and flight-path angle to initiate the inward spiral. On the other hand, the three trials with $R_{\min} = 50$, 30, and 10 Earth radii show that the vehicle has intersected the boundary curve beyond the required orbital position, and, therefore, a significant coasting arc (greater than 180 deg) is necessary. Lunar and solar gravitational effects will perturb the orbit during the coast phase, and the onboard guidance system could monitor the vehicle's osculating orbital elements and initiate the inward spiral phase at the appropriate conditions. Table 3 also presents the duration of the yaw-steering phase $t_\beta$ and the final inclination at interception of the Perkins boundary. The time required for the yaw-steering phase (with 25-deg inclination change) is relatively short (7–10 days), and the yaw phase occurs

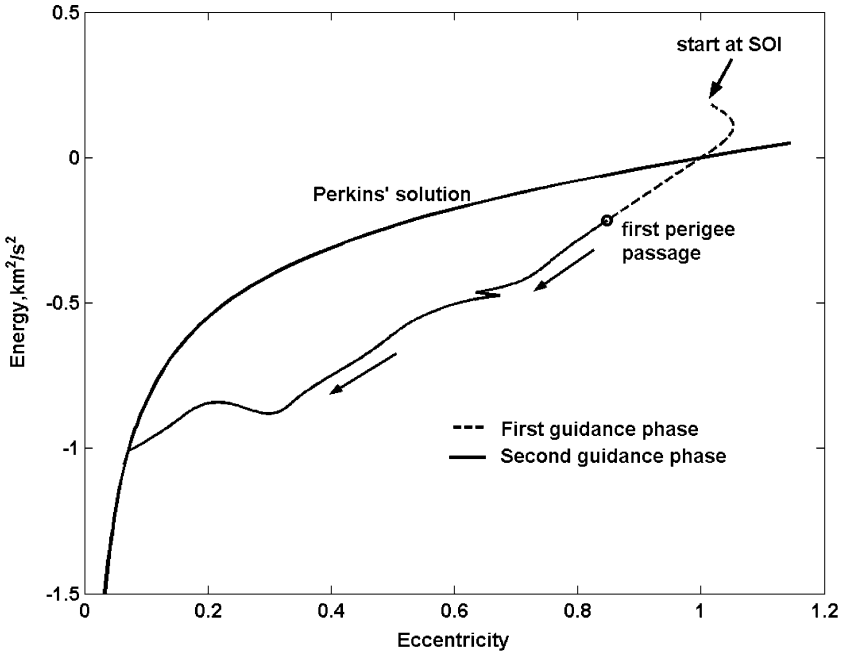


**Fig. 7 Guided trajectory in energy–eccentricity space from SOI to spiral target boundary.**

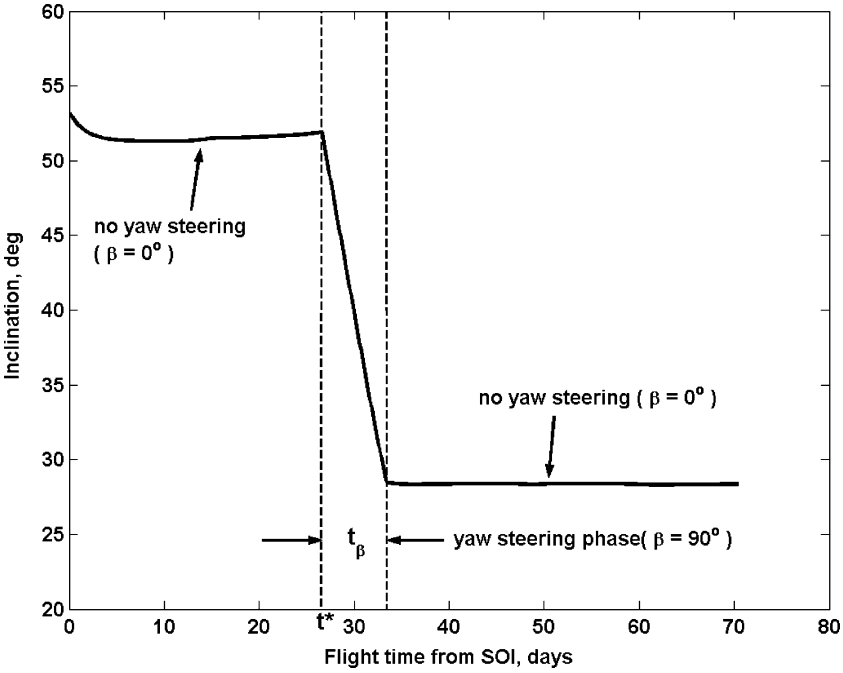


**Fig. 8 Inclination history from SOI to spiral target boundary.**

near apogee. As a final note, Table 3 shows that the total powered time from first perigee passage to LEO, that is, $t_{G2} + t_{\text{spiral}}$, is between 231 to 248 days, and that the total powered time increases as $R_{\min}$ (energy threshold) decreases.

Figure 7 shows the guided trajectory from the initial conditions (near SOI) to the spiral target boundary, as presented in the energy–eccentricity space. The trajectory shown in Fig. 7 uses a lower radius bound of 30 $Re$ for the second guidance phase. The dashed arc represents the initial guidance phase (SOI to first perigee passage), and the solid arc represents the second guidance phase (perigee to spiral target). Note that eccentricity initially increases during the first guidance phase until it reaches a maximum value and is then reduced to 0.847 at perigee. In general, energy and eccentricity steadily decrease during the second guidance phase as the spacecraft reaches the Perkins's solution boundary. Note that a zig-zag in energy and eccentricity occurs when eccentricity is near 0.65. This deviation is a result of the yaw-steering phase, when no thrust component is in the orbit plane ($\beta = 90$ deg) and the orbit is perturbed by third-body effects. Figure 8 presents the inclination change during the capture maneuver. Third-body perturbation effects are noticeable during the start of the capture, and the seven-day yaw-steering phase quickly reduces inclination to the desired value of 28.5 deg. Figure 9 presents the pitch and yaw steering programs, $\alpha(t)$ and $\beta(t)$, during the powered capture to the Perkins's boundary. Discontinuities in the pitch program mark the guidance updates to $\lambda$ during the first guidance phase ($t < 15.7$ days). Note that pitch angle is near $\pm 90$ deg when the yaw-steering phase is employed. (Here, $\mathrm{d}i/\mathrm{d}t$ is maximized because the spacecraft is in the vicinity of apogee and the nodal crossing.)

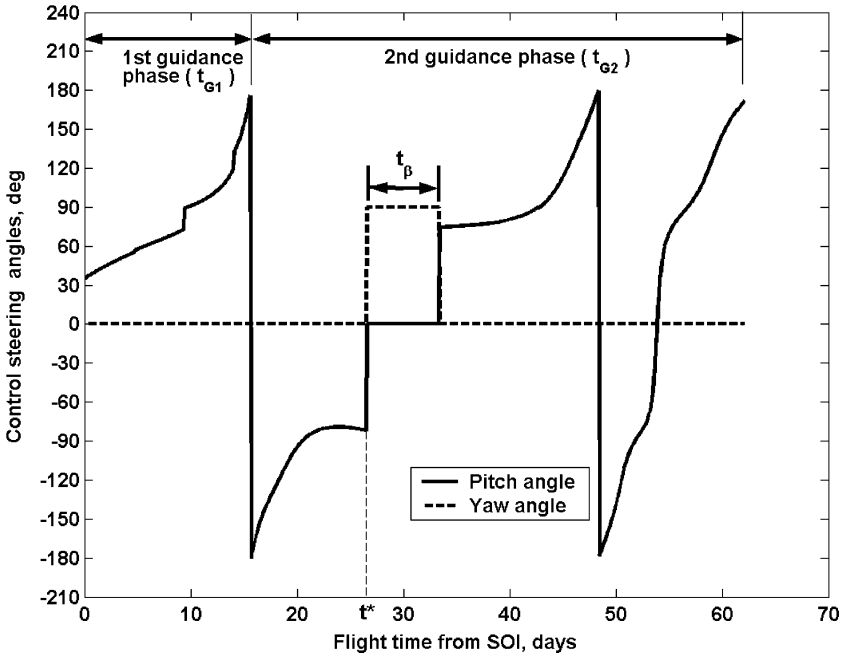


**Fig. 9 Steering programs from SOI to spiral target boundary.**

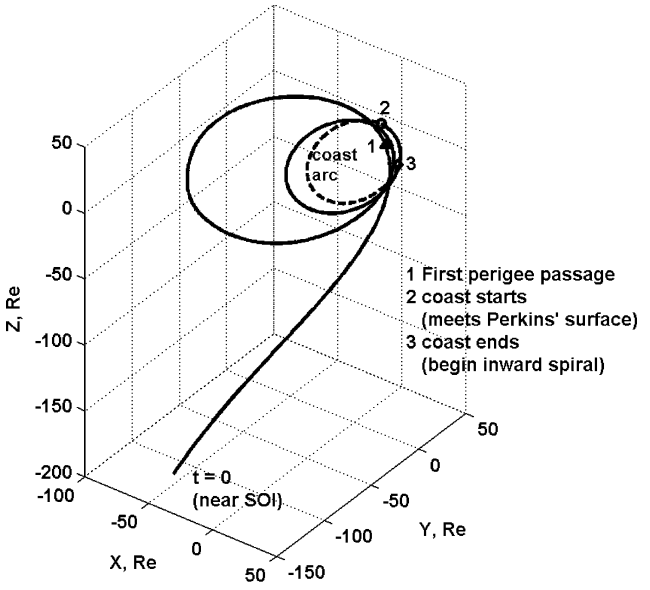


**Fig. 10 Three-dimensional SEP Earth-capture trajectory.**

Radial thrust on both sides of the yaw phase exists because the guidance parameter $\lambda$ is approximately unity, and the horizontal components of the two steering laws essentially cancel [c.f. Eqs. (9), (10), (17), and (18)], leaving a component along the radial direction. Radial thrust near apogee has a small effect on both energy and eccentricity, and so switching to pure out-of-plane steering is a beneficial strategy. Figure 10 presents the three-dimensional capture trajectory, and shows that the SEP spacecraft completes about 2.5 revolutions during the capture trajectory to Perkins's boundary (point 2). The coast arc to the proper inward spiral (the inner arc on Fig. 10) requires more than three-quarters of a revolution.

We computed additional guided capture simulations to determine the maximum possible energy at the SOI that still permits capture before the first perigee passage. To do this, we increased the magnitude of the velocity at the SOI $\boldsymbol{v}_0$ and maintained the original velocity direction and initial position vector $\boldsymbol{r}_0$ as shown in Table 1. We found that the guidance scheme and SEP configuration used in this paper were able to achieve capture at first perigee for velocity increases as high as 20% greater than the nominal value in Table 1. Note that a 20% increase in velocity at the SOI corresponds to a 44% increase in orbital energy.

## Conclusions

A new guidance scheme for Earth-capture trajectories that uses low-thrust propulsion has been developed. The guidance design divides the capture maneuver into three phases: 1) initial energy and eccentricity reduction, 2) transition to spiral boundary surface, and 3) spiral transfer to target LEO. Thrust steering programs for the first two phases are based on a linear combination of two control laws that reduce energy and eccentricity. The control laws are blended by the use of a single guidance parameter, $\lambda$. During the initial phase, the guidance algorithm iterates on the guidance parameter such that eccentricity is minimized at the first perigee passage. During the second phase, the guidance algorithm adjusts the parameter $\lambda$, so that the projected trajectory reaches an energy–eccentricity state that ensures a subsequent quasi-circular inward spiral to LEO. In addition, the guidance scheme predicts the best time to switch to out-of-plane steering to maximize the inclination rate. Once the vehicle has reached the spiral target state, a simple antitangent steering profile can be used to guide the spacecraft to LEO.

The capture guidance algorithm is demonstrated by several numerical examples that show that the scheme can successfully guide a spacecraft from an incoming radial hyperbolic trajectory to a stable, nearly circular orbit. Note that a fully end-to-end optimized trajectory may result in a flight path at the sphere of influence that is far from radial. However, our proposed scheme should be capable of successfully guiding the spacecraft for these cases with more benign initial flight paths. In addition, an optimal end-to-end trajectory may take advantage of a lunar gravity assist during capture. However, unforeseen anomalies (such as changes in thruster performance) may make such a complex, preplanned maneuver unattainable, whereas our proposed scheme would be capable of guiding the vehicle to a stable closed orbit.

The guidance design is simple, reliable, and can be implemented onboard for autonomous operation. Our technique makes novel use of Perkins's universal low-thrust spiral trajectory solutions as a convenient target state. The choice of control laws coupled with the spiral trajectory boundary target provides a robust method for guiding the vehicle from a high-energy trajectory to a benign inward

spiral mode. The simplicity and performance of our guidance design makes it a viable candidate for onboard implementation.

## References

[1]Rayman, M. D., Varghese, P., Lehman, D. H., and Livesay, L. L., "Results from the Deep Space 1 Technology Validation Missions," *Acta Astronautica*, Vol. 47, Nos. 2–9, 2000, pp. 475–487.

[2]Vadali, S. R., Aroonwilairut, K., and Braden, E., "A Hybrid Trajectory Optimization Technique for the Mars Sample Return Mission," *Advances in the Astronautical Sciences*, Vol. 109, American Astronautical Society, San Diego, 2001, pp. 2309–2320.

[3]Battin, R. H., *Astronautical Guidance*, 1st ed., McGraw–Hill, New York, 1964, pp. 344–354.

[4]Whiffen, G. J., and Sims, J. A., "Application of the SDC Optimal Control Algorithm to Low-Thrust Escape and Capture Trajectory Optimization," *Advances in the Astronautical Sciences*, Vol. 112, American Astronautical Society, San Diego, 2002, pp. 1361–1382.

[5]Whiffen, G. J., and Sims, J. A., "Application of the SDC Optimal Control Algorithm to Low-Thrust Escape and Capture Including Fourth Body Effects," 2nd International Symposium on Low Thrust Trajectories, Centre National d'Etudes Spatiales, Paper 02-20, Toulouse, France, June 2002.

[6]Kluever, C. A., "Optimal Earth-Capture Trajectories Using Electric Propulsion," *Journal of Guidance, Control, and Dynamics*, Vol. 25, No. 3, 2002, pp. 604–606.

[7]Petropoulos, A. E., "Simple Control Laws for Low-Thrust Orbit Transfers," American Astronautical Society, AAS Paper 03-630, Aug. 2003.

[8]Desai, S. D., Bhaskaran, S., Bollman, W. E., Halsell, C. A., Riedel, J. E., and Synnott, S. P., "The DS-1 Autonomous Navigation System: Autonomous Control of Low Thrust Propulsion Systems," AIAA Paper 97-38819, Aug. 1997.

[9]Perkins, F. M., "Flight Mechanics of Low-Thrust Spacecraft," *Journal of the Aerospace Sciences*, Vol. 26, No. 5, 1959, pp. 291–297.

[10]Bate, R. R., Mueller, D. D., and White, J. E., *Fundamentals of Astrodynamics*, Dover, New York, 1971, pp. 387–390.

[11]Spitzer, A., "Near Optimal Transfer Orbit Trajectory Using Electric Propulsion," *Advances in the Astronautical Sciences*, Vol. 89, American Astronautical Society, San Diego, 1995, pp. 1031–1044.